The Generalized Dirichlet-Neumann Map for Linear Elliptic PDEs and its Numerical Implementation ⋆

A.G.Sifalakis[1], A.S.Fokas[2], S.R.Fulton[3] and Y.G.Saridakis[1, *]

[1] *Applied Mathematics and Computers Lab, Department of Sciences, Technical University of Crete, 73100 Chania, Greece*

[2] *Department of Applied Mathematics and Theoretical Physics, University of Cambridge, Cambridge CB3 0WA, United Kingdom*

[3] *Department of Mathematics and Computer Science, Clarkson University, Potsdam NY 13699-5815, USA*

Abstract

A new approach for analyzing boundary value problems for linear and for integrable nonlinear PDEs was introduced in [1]. For linear elliptic PDEs, an important aspect of this approach is the characterization of a generalized Dirichlet to Neumann map: given the derivative of the solution along a direction of an arbitrary angle to the boundary, the derivative of the solution perpendicularly to this direction is computed *without* solving on the interior of the domain. This is based on the analysis of the so-called *global relation*, an equation which couples known and unknown components of the derivative on the boundary and which is valid for all values of a complex parameter k. A collocation-type numerical method for solving the *global relation* for the Laplace equation in an arbitrary bounded convex polygon was introduced in [2]. Here, by choosing a different set of the *"collocation points"* (values for k), we present a significant improvement of the results in [2]. The new collocation points lead to well conditioned collocation methods. Their combination with sine basis functions leads to a collocation matrix whose diagonal blocks are point diagonal matrices yielding efficient implementation of iterative methods; numerical experimentation suggests quadratic convergence. The choice of Chebyshev basis functions leads to higher order convergence, which for regular polygons appear to be exponential.

Key words : elliptic PDEs, Dirichlet-Neumann map, global relation, collocation, iterative methods

2000 MSC : 35J25, 65N35, 64N99, 65F05, 65F10

⋆ This work was supported by the Greek Ministry's of Education *EPEAEK-Herakleitos* grand which is partially funded by the EU

* Corresponding author. E-mail : yiannis@science.tuc.gr

1 Introduction

A new approach for analyzing boundary value problems for linear and for integrable nonlinear PDEs in two dimensions was introduced in [1],[3]. This approach was developed by several researchers, and has led to the emergence of a new method for solving boundary value problems. This method involves two novel features:

(a) It yields an analytic representation of the solution in the form of an integral in the complex k-plane.

(b) It characterizes a generalized Dirichlet to Neumann map through the solution of the so-called *global relation*, which is an equation valid for all complex values of k, which couples specified and unknown values of the solution and its derivatives on the boundary.

For a large class of boundary value problems, the global relation can be solved analytically, and hence the generalized Dirichlet to Neumann map can be constructed in closed form. This includes linear evolution PDEs with spatial derivatives of arbitrary order on the half-line [4] and on a finite interval [5], the Laplace, the bi-harmonic and the modified Helmholtz equation in certain simple polygons [6] - [9], and the basic nonlinear integrable evolution PDEs on the half-line for certain simple boundary conditions [10]-[11]. However, for general boundary value problems, the global relation must be solved numerically.

The implementation of the new method to the case of the Laplace equation in an arbitrary bounded convex polygon was presented in [2], where :

(a) It was shown that the global relation is not only a necessary but also a sufficient condition for existence. This reduces the problem of solving Laplace's equation, to the problem of solving the global relation.

(b) A collocation-type numerical method was introduced for solving the global relation. This method is based on evaluating both the real and imaginary parts of the global relation at the following values of the complex parameter k *("collocation points")*:

$$k = -\frac{l}{h_p}, \quad h_p = \frac{1}{2\pi}\left(z_{p+1} - z_p\right), \quad p = 1, 2, \ldots, n, \quad l = 1, 2, \ldots, \frac{N}{2}, \tag{1.1}$$

where n is the number of the sides of the polygon, $\{z_i\}_{i=1}^{n}$ are the corners of the polygon in the complex z-plane (with $z_{n+1} = z_1$), and N, which is chosen to be even, is the number of points used for the discrete approximation of the unknown boundary values. This choice has been motivated by the analytical integral representation in [3] (see also Remark 2.1).

In this paper, aiming to improve and stabilize the order of convergence and the associated conditioning number of the collocation method in [2], we use a different

set of *collocation points* (the values of the complex parameter k): we use the values specified by equations (1.1) for the *imaginary part* of the global relation, but we choose the values

$$l = \frac{1}{2}, \frac{3}{2}, \frac{5}{2}, \ldots, \frac{N-1}{2} \quad , \tag{1.2}$$

for the *real part* of the global relation.

The above choice, for sine basis functions, yields a linear algebraic system whose diagonal blocks of the associated coefficient matrix are point diagonal matrices. That is, the collocation coefficient matrix is by construction *block-Jacobi preconditioned*, pointing directly to the efficient implementation of iterative techniques. Numerical investigation suggests a quadratically convergent and well conditioned collocation method. The classical Jacobi and Gauss-Seidel as well as the BiCGstab iterative techniques converge rapidly, yielding the solution after only a few iterations. The rate of convergence can be improved by choosing a different set of basis functions. In particular, for Chebyshev basis functions, numerical experiments suggest that, for regular polygons, the convergence is exponential.

This paper is organized as follows: Section 2 outlines some of the analytical results of [2]. Section 3 presents the details of the new numerical solution of the global relation and explains the choice of the new collocation points. Section 4 presents numerical results for a variety of domains with different boundary conditions, and compares these results with the analogous results of [2]. Section 5 discusses further these results.

2 Overview

For elliptic PDEs in two dimensions x and y, it is convenient to replace the Cartesian coordinates x and y with the complex coordinates z and $\bar{z}$,

$$z = x + iy, \quad \bar{z} = x - iy \; . \tag{2.1}$$

Using the equations

$$\partial_z = \frac{1}{2}\left(\partial_x - i\partial_y\right) \; , \quad \partial_{\bar{z}} = \frac{1}{2}\left(\partial_x + i\partial_y\right) \; ,$$

it follows that the Laplace equation in the independent variable q can be rewritten in the form

$$\frac{\partial^2 q}{\partial z \partial \bar{z}} = 0. \tag{2.2}$$

This equation is equivalent to the equation

$$\frac{\partial}{\partial \bar{z}}\left(e^{-ikz}\frac{\partial q}{\partial z}\right)=0, \tag{2.3}$$

for an *arbitrary* complex parameter k.

Suppose that the real-valued function $q(z,\bar{z})$ satisfies Laplace's equation (2.2) in a simply connected bounded domain D with boundary ∂D. Then, equation (2.3) together with the complex form of Green's theorem imply the equation

$$\int_{\partial D} e^{-ikz}\frac{\partial q}{\partial z}dz=0, \quad k\in\mathbb{C}\,. \tag{2.4}$$

Following [3] we shall refer to equation (2.4) as the *global relation* associated with Laplace's equation.

Suppose that $q(z,\bar{z})$ satisfies the Laplace's equation in a convex bounded polygon with vertices $z_1, z_2, \ldots, z_n$ (modulo n), which have indexed counter-clockwise, see Figure 2.1. Then the global relation (2.4) becomes

$$\sum_{j=1}^{n}\int_{S_j} e^{-ikz}\frac{\partial q}{\partial z}dz=0, \quad k\in\mathbb{C}\,, \tag{2.5}$$

where S_j denotes the side from z_j to z_{j+1} (not including the end points).

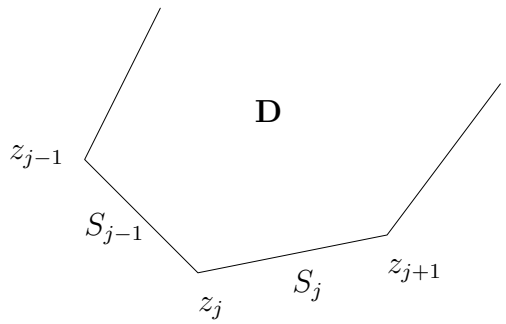

Figure 2.1 Part of the bounded convex polygon with vertices z_j, sides S_j, and interior D.

Proposition 2.1 *Let the real-valued function $q(z,\bar{z})$ satisfy the Laplace equation in the interior D of the polygon with corners $\{z_i\}_{i=1}^{n}$ depicted in Figure 2.1. Let $g^{(j)}$ denote the derivative of the solution in the direction making an angle β_j, $0\le\beta_j\le\pi$, with the side S_j, i.e.*

$$\cos(\beta_j)\,q_s^{(j)}+\sin(\beta_j)\,q_n^{(j)}=g^{(j)}, \quad z\in S_j, \quad 1\le j\le n, \tag{2.6}$$

where $q_s^{(j)}$ *and* $q_n^{(j)}$ *denote the tangential and (outward) normal components of* $\dfrac{\partial q}{\partial z}$ *along the side* S_j*. Let* $f^{(j)}$ *denote the derivative of the solution in the direction normal to the above direction, i.e.*

$$-\sin(\beta_j)\, q_s^{(j)} + \cos(\beta_j)\, q_n^{(j)} = f^{(j)}, \quad z \in S_j, \quad 1 \le j \le n. \tag{2.7}$$

The generalized Dirichlet-Neumann map, i.e. the relation between the sets $\left\{f^{(j)}\right\}_{j=1}^{n}$ *and* $\left\{g^{(j)}\right\}_{j=1}^{n}$*, is characterized by the single equation*

$$\sum_{j=1}^{n} |h_j|\, e^{i(\beta_j - k m_j)} \int_{-\pi}^{\pi} e^{-ikh_j s} \left(f^{(j)}(s) - i g^{(j)}(s)\right) ds = 0, \quad k \in \mathbb{C}\,, \tag{2.8}$$

where

$$h_j := \frac{1}{2\pi}\,(z_{j+1} - z_j)\,, \quad m_j := \frac{1}{2}\,(z_{j+1} + z_j)\,, \quad j = 1, 2, \ldots, n, \quad z_{n+1} = z_1. \tag{2.9}$$

Evaluating equation (2.8) on the following n-rays of the complex k-plane

$$k_p = -\frac{l}{h_p}, \quad l \in \mathbb{R}^+, \quad p = 1, \ldots, n\,, \tag{2.10}$$

and multiplying the resulting equations by $\exp\left[-i(\beta_p + l m_p/h_p)\right] / |h_p|$*, equation (2.8) yields the following set of n equations:*

$$\sum_{j=1}^{n} \frac{|h_j|}{|h_p|} e^{i(\beta_j - \beta_p)} e^{-\frac{il}{h_p}(m_p - m_j)} \int_{-\pi}^{\pi} e^{il\frac{h_j}{h_p}s} \left(f^{(j)}(s) - i g^{(j)}(s)\right) ds = 0, \quad l \in \mathbb{R}^+, \quad p = 1, \ldots, n\,. \tag{2.11}$$

Proof: Let a_j denote the angle of the side S_j with the horizontal axis i.e.

$$a_j = \arg(z_{j+1} - z_j)\,, \quad h_j = |h_j|\, e^{i a_j}\,. \tag{2.12}$$

Equations (2.6) and (2.7) can be considered as two equations expressing $q_s^{(j)}$ and $q_n^{(j)}$ in terms of $g^{(j)}$ and $f^{(j)}$,

$$\begin{aligned} q_n^{(j)} &= \sin(\beta_j)\, g^{(j)} + \cos(\beta_j)\, f^{(j)}\,, \\ q_s^{(j)} &= \cos(\beta_j)\, g^{(j)} - \sin(\beta_j)\, f^{(j)}\,. \end{aligned}$$

Substituting these expressions in the identity

$$\frac{\partial q^{(j)}}{\partial z} = \frac{1}{2} e^{-i a_j} \left(q_s^{(j)} + i q_n^{(j)}\right),$$

we find

$$\frac{\partial q^{(j)}}{\partial z} = \frac{1}{2} e^{-i(a_j - \beta_j)} \left(g^{(j)} + i f^{(j)} \right). \tag{2.13}$$

In order to evaluate the integral of the expression $\exp[-ikz]\, \partial q^{(j)}/\partial z$ along the side S_j, we introduce the following local coordinates: For $z \in S_j$, we let

$$z = \frac{1}{2}(z_j + z_{j+1}) + \frac{s}{2\pi}(z_{j+1} - z_j), \quad -\pi < s < \pi.$$

Note that for $s = -\pi$ and π, $z = z_i$ and z_{i+1}, respectively. Writing the above expression in terms of h_j and m_j, we find

$$z = m_j + s h_j. \tag{2.14}$$

Substituting the expressions for z and $\partial q^{(j)}/\partial z$ from equations (2.14) and (2.13) into the global relation (2.5), and multiplying the resulting equation by $-i$ we find equation (2.8). ■

Remark 2.1 Suppose that the set $\left\{g^{(j)}\right\}_{j=1}^{n}$ is known. Then, equation (2.8) is a *single* equation for the n unknown functions $\left\{f^{(j)}(s)\right\}_{j=1}^{n}$. However, this equation is valid for *all* complex values of k. Thus, it is possible to generate a multitude of equations from the single equation (2.8), by prescribing a multitude of values for k. It is shown in [2] that a convenient choice for these values is the one defined in equations (2.10). This choice can be motivated as follows: Suppose we only had one unknown $f^{(p)}$. Then, we would choose k in such a way that kh_p is real, i.e. $kh_p = -l$ or $kh_p = l$. The latter choice coincides with the values of k appearing in the analytical integral representation (see [3]). However, the integral representation involves e^{ikz} whereas the global relation involves e^{-ikz}, thus we now choose $kh_p = -l$.

Remark 2.2 In what follows we assume that $g^{(j)}$ are compatible in the corners and we seek a solution in the function class specified in [2].

Remark 2.3 The end values of the unknown functions $f^{(j)}$ can be calculated by the continuitity requirements $q_z^{(j)}(z_j) = q_z^{(j-1)}(z_j)$. Namely, using the expression (2.13) and setting $\delta_j = a_j - \beta_j$ we obtain (see also [2])

$$f^{(j)}(\pi) = \frac{\cos(\delta_{j+1} - \delta_j)\, g^{(j)}(\pi) - g^{(j+1)}(\pi)}{\sin(\delta_{j+1} - \delta_j)},$$

$$f^{(j)}(-\pi) = \frac{g^{(j-1)}(\pi) - \cos(\delta_j - \delta_{j-1})\, g^{(j)}(-\pi)}{\sin(\delta_j - \delta_{j-1})}.$$

3 The Numerical Method

Proposition 3.1 *The generalized Dirichlet-Neumann map is defined by proposition 2.1. Suppose that the set* $\left\{g^{(j)}\right\}_{j=1}^{n}$ *is given. Suppose that* $f^{(j)}(s)$ *is approximated by*

$$f_N^{(j)}(s) = f_*^{(j)}(s) + \sum_{r=1}^{N} U_r^j \varphi_r(s), \quad j = 1, \ldots, n, \quad N \text{ even integer}, \tag{3.1}$$

where $\varphi_r(s)$ *are appropriate basis functions and*

$$f_*^{(j)}(s) = \frac{1}{2\pi}\left[(s+\pi) f^{(j)}(\pi) - (s-\pi) f^{(j)}(-\pi)\right].$$

Then, the real coefficients U_r^j *satisfy the* Nn *algebraic set of equations*

$$\sum_{j=1}^{n} \frac{|h_j|}{|h_p|} e^{i(\beta_j - \beta_p)} e^{-i\frac{l}{h_p}(m_p - m_j)} \sum_{r=1}^{N} U_r^j F_r\left(\frac{l h_j}{h_p}\right) = G_p(l), \quad p = 1, 2, \ldots, n, \tag{3.2}$$

where $G_p(l)$ *denotes the known function*

$$G_p(l) = i \sum_{j=1}^{n} \frac{|h_j|}{|h_p|} e^{i(\beta_j - \beta_p)} e^{-i\frac{l}{h_p}(m_p - m_j)} \int_{-\pi}^{\pi} e^{il\frac{h_j}{h_p}s} (g^{(j)}(s) + i f_*^{(j)}(s)) ds, \tag{3.3}$$

$F_r(l)$ *denotes the integral*

$$F_r(l) = \int_{-\pi}^{\pi} e^{ils} \varphi_r(s) ds, \quad r = 1, 2, \ldots, N, \tag{3.4}$$

and l *is chosen as follows: For the imaginary part of equations (3.2)* $l = 1, 2, \ldots, N/2$, *whereas for the real part of equations (3.2) ,* $l = \frac{1}{2}, \frac{3}{2}, \ldots, \frac{N-1}{2}$.

In the particular case that $\varphi_r(s)$ *are the sine basis functions, that is*

$$\varphi_r(s) = \sin\left[r\left(\frac{\pi + s}{2}\right)\right], \quad r = 1, 2, \ldots, N, \tag{3.5}$$

the term $j = p$ in the summation of the left hand side of equations (3.2) is given by the following:

$$\begin{array}{llll} l = \frac{1}{2}: & \pi U_1^p & l = 1: & -\pi U_2^p \\ l = \frac{3}{2}: & -\pi U_3^p & l = 2: & \pi U_4^p \\ l = \frac{5}{2}: & \pi U_5^p & l = 3: & -\pi U_6^p \\ \vdots & & \vdots & \end{array} \tag{3.6}$$

Proof: Substituting the representation (3.1) in equations (2.11) we find equations (3.2).

The term $j = p$ in the summation of the left hand side of equations (3.2) is given by

$$\sum_{r=1}^{N} U_r^j F_r(l) = \sum_{r=1}^{N} U_r^j R_r(l) + i \sum_{r=1}^{N} U_r^j I_r(l), \tag{3.7}$$

where $R_r(l)$ and $I_r(l)$ denote the real and imaginary parts of the integral $F_r(l)$ defined by equation (3.4). Let δ_{ab} denote the Kronecker function. Using

$$\begin{gathered} R_r\left(\frac{1}{2}\right) = \pi\delta_{r1}, \quad R_r\left(\frac{3}{2}\right) = -\pi\delta_{r3}, \quad R_r\left(\frac{5}{2}\right) = \pi\delta_{r5}, \quad \cdots \\ I_r(1) = -\pi\delta_{r2}, \quad I_r(2) = \pi\delta_{r4}, \quad I_r(4) = -\pi\delta_{r8}, \quad \cdots \end{gathered}$$

equation (3.7) yields the expressions (3.6). ■

Remark 3.1 To explain the choice of the new collocation points let us isolate one of the unknown integrals in the global relation (2.11) and denote by $H_p(k)$ the remaning terms,

$$\int_{-\pi}^{\pi} e^{i|k||h_p|s} f^{(p)}(s) ds = H_p(k), \quad k = |k| e^{i(\pi - \alpha_p)}, \quad p = 1, \ldots, n\,. \tag{3.8}$$

The complex conjugate of this equation yields

$$\int_{-\pi}^{\pi} e^{-i|k||h_p|s} f^{(p)}(s) ds = \bar{H}_p(k), \quad k = |k| e^{i(\pi + \alpha_p)}, \quad p = 1, \ldots, n\,. \tag{3.9}$$

The left hand sides of equations (3.8)-(3.9) involve both sines and cosines. However, since $f^{(p)}(s)$ vanishes at the end points we seek integral representations involving only sines. Thus we let $s = 2t - \pi$ in equations (3.8)-(3.9) and we find the following equations:

$$2\int_0^{\pi} [cos(2|k||h_p|t) + isin(2|k||h_p|t)]f^{(p)}(2t-\pi)dt = e^{i|k||h_p|\pi} H_p(-|k|e^{-i\alpha_p)},$$

$$2\int_0^{\pi} [cos(2|k||h_p|t) - isin(2|k||h_p|t)]f^{(p)}(2t-\pi)dt = e^{-i|k||h_p|\pi} \bar{H}_p(-|k|e^{i\alpha_p)}.$$

Subtracting these equations and letting

$$2|k||h_p| = l, \quad l = 1, 2, \ldots$$

we find

$$4i\int_0^{\pi} sin(lt)f^{(p)}(2t-\pi)dt = e^{\frac{il\pi}{2}} H_p(-\frac{l}{2h_p}) - e^{\frac{-il\pi}{2}} \bar{H}_p(-\frac{l}{2\bar{h}_p}), \tag{3.10}$$

for $l = 1, 2, \ldots,$ and $p = 1, \ldots, n$. Taking $e^{\frac{il\pi}{2}}$ as a common factor and using the fact that $e^{-il\pi}$ equals -1 if l is odd and 1 if l is even, whereas $e^{\frac{il\pi}{2}}$ equals $(-1)^{l/2}$ if l is even equation (3.10) becomes

$$4\int_0^{\pi} sin(lt)f^{(p)}(2t-\pi)dt = \begin{cases} (-1)^{(l-1)/2}[H_p(-\frac{l}{2h_p}) + \bar{H}_p(-\frac{l}{2\bar{h}_p})], & l \text{ odd}, \\ (-1)^{l/2}[H_p(-\frac{l}{2h_p}) - \bar{H}_p(-\frac{l}{2\bar{h}_p})], & l \text{ even}. \end{cases}$$

4 Numerical Results

Following directly Proposition 3.1, we construct the $Nn \times Nn$ linear system of equations, defined by relations (3.2)-(3.6), needed to determine the Nn unknown coefficients U_r^j in (3.1). Relation (3.2), which is the discrete analogue of the global relation (2.11), is a complex system of n equations. By choosing $\frac{N}{2}$ values of l for the real part of these equations and $\frac{N}{2}$ values of l for the imaginary part, we obtain a system of Nn real equations.

4.1 Comparison of SFFS and FFX methods for sine basis functions

The choice for the values of l specified in Proposition 3.1, in the case of sine basis functions, leads to a system whose coefficient matrix has the structure shown schematically in Figure 4.1a, that is the $N \times N$ block diagonal submatrices are

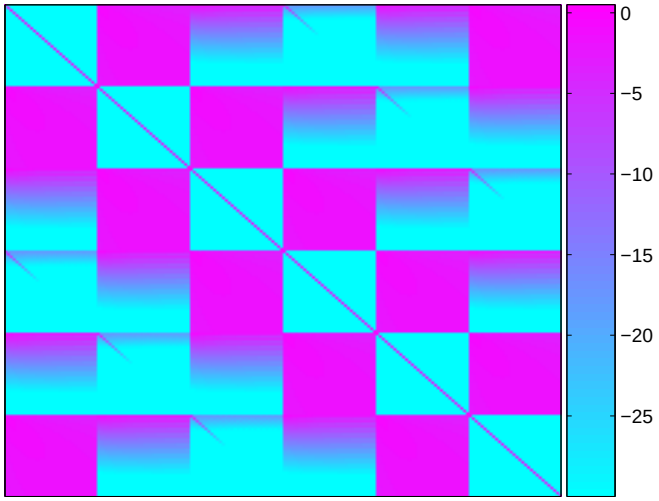

(a)

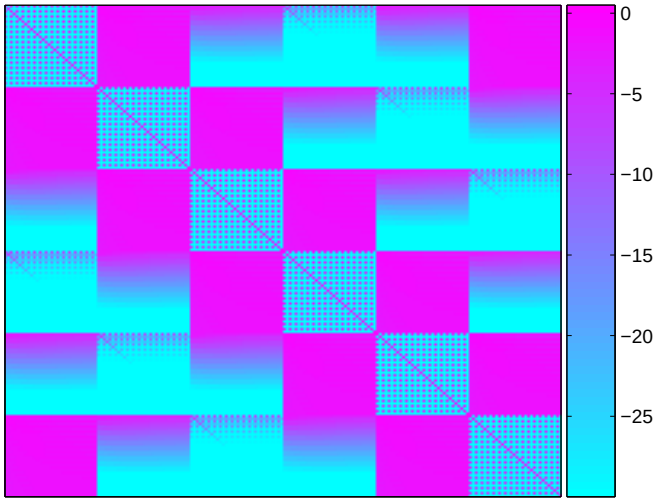

(b)

Figure 4.1 The structures of the coefficient matrices produced (a) by Proposition 3.1 (SFFS method) and (b) in [2] (FFX method), for $n = 6$ and $N = 32$

diagonal matrices. This should be compared to the block structure of the matrix obtained in [2] for the *physical space* case which is shown in Figure 4.1b.

To illustrate the numerical implementation of the method, as well as to compare with the one presented in [2], we apply it to the Laplace equation for a variety of regular and irregular polygon domains with Dirichlet, Neumann and Mixed ($\frac{\pi}{3}$) boundary conditions. In all cases the exact solution of the Laplace equation is given

by

$$q(x,y) = \sinh(3x)\sin(3y)\ , \tag{4.1}$$

and the corresponding boundary conditions as well as the corresponding functions $\left\{f^{(j)}(s)\right\}_{j=1}^{n}$ and $\left\{g^{(j)}(s)\right\}_{j=1}^{n}$ can be generated analytically. The relative error E_∞, used to demonstrate the performance of the methods, is given by

$$E_\infty = \frac{||f - f_N||_\infty}{||f||_\infty}\ , \tag{4.2}$$

where

$$||f||_\infty = \max_{1\le j\le n}\left\{\max_{-\pi\le s\le\pi}|f^{(j)}(s)|\right\} \tag{4.3}$$

and

$$||f - f_N||_\infty = \max_{1\le j\le n}\left\{\max_{-\pi\le s\le\pi}|f^{(j)}(s) - f_N^{(j)}(s)|\right\}, \tag{4.4}$$

with $f_N^{(j)}$ as in (3.1), and the max over s is taken over a dense discretization of the interval $[-\pi,\pi]$. The number N of basis functions on each side remains the same in all experiments and takes successively the values $N = 4, 8, 16, 32, 64, 128, 256$. For the direct solution of the linear systems we have used the standard LAPACK routines, while for the computation of the right hand side vector we have used a routine (*dqawo*) from QUADPACK implementing the modified Clenshaw-Curtis technique.

Figures 4.2, 4.3 and 4.4 refer to the solution for *regular* polygons with Dirichlet ($\beta_j = 0$), Neumann ($\beta_j = \frac{\pi}{2}$) and Mixed ($\beta_j = \frac{\pi}{3}$) boundary conditions respectively. The vertices z_j of the regular n-gons used in our experiments are lying on a circle centered at the origin with radius $\sqrt{2}$ and they are given by

$$z_j = \sqrt{2}e^{i[2(j-1)\frac{\pi}{n} - \frac{1}{5}]}\ , \quad j = 1,\ldots,n\ .$$

The dotted, dashed and dash-dotted lines in the figures are the lines $\frac{1}{N}$, $\frac{1}{N^2}$ and $\frac{1}{N^3}$ indicating the slopes for convergence of order 1, 2 and 3 respectively. We note that in all cases both methods converge. However, the errors produced by the method described in Proposition 3.1 (SFFS) are significantly smaller.

Furthermore, one may easily observe that the error lines for the SFFS method are parallel to the $\frac{1}{N^2}$ line indicating a quadratically convergent method with respect to the infinity error norm. To highlight this fact, the order of convergence (O.o.C) of both methods, for several cases of regular polygons, has been numerically estimated and included in Tables 4.1-4.4 that follow.

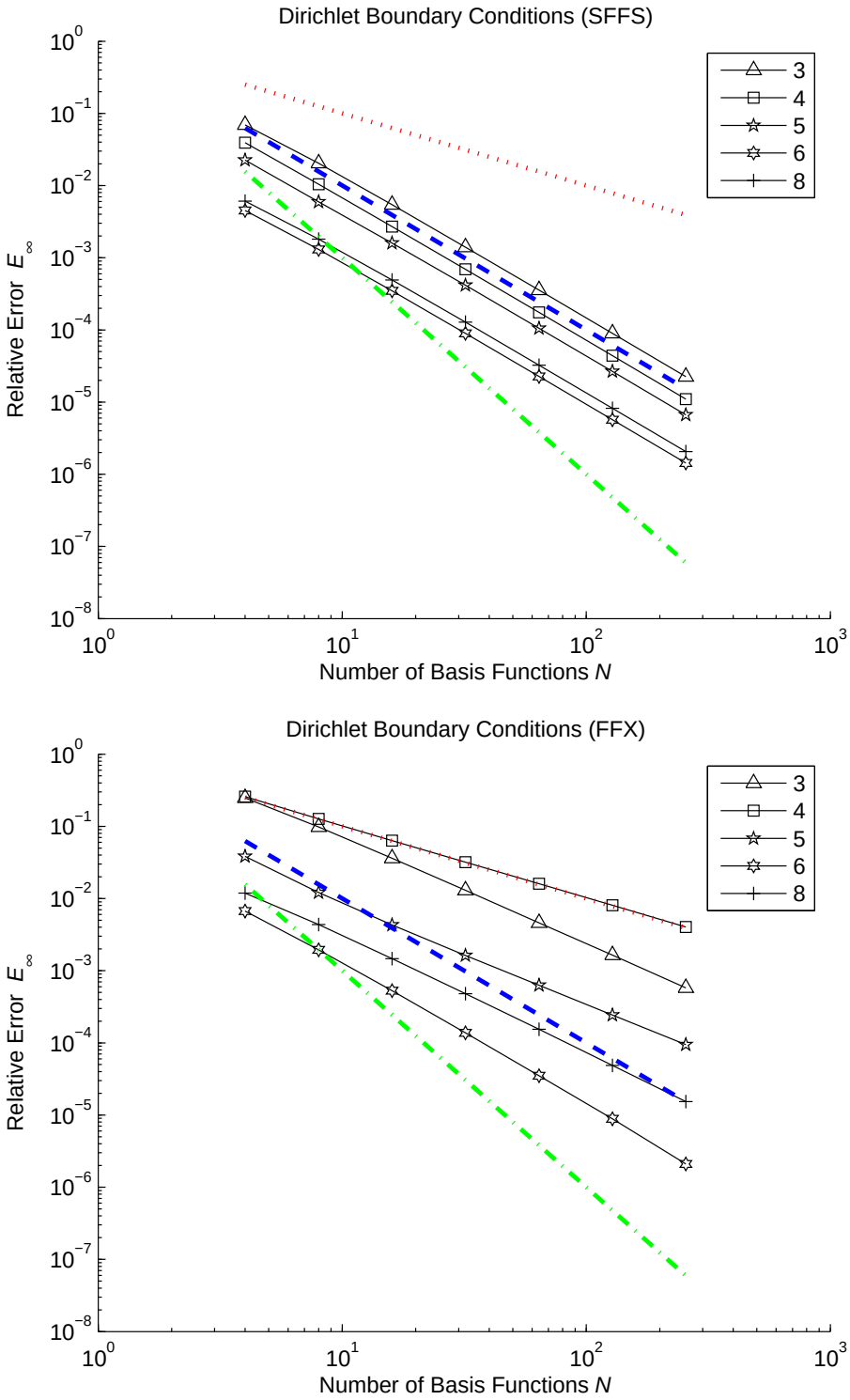

Figure 4.2 Case of regular polygons and Dirichlet boundary conditions : E_∞ as a function of N for the method presented here (SFFS) and the method presented in [2] (FFX)

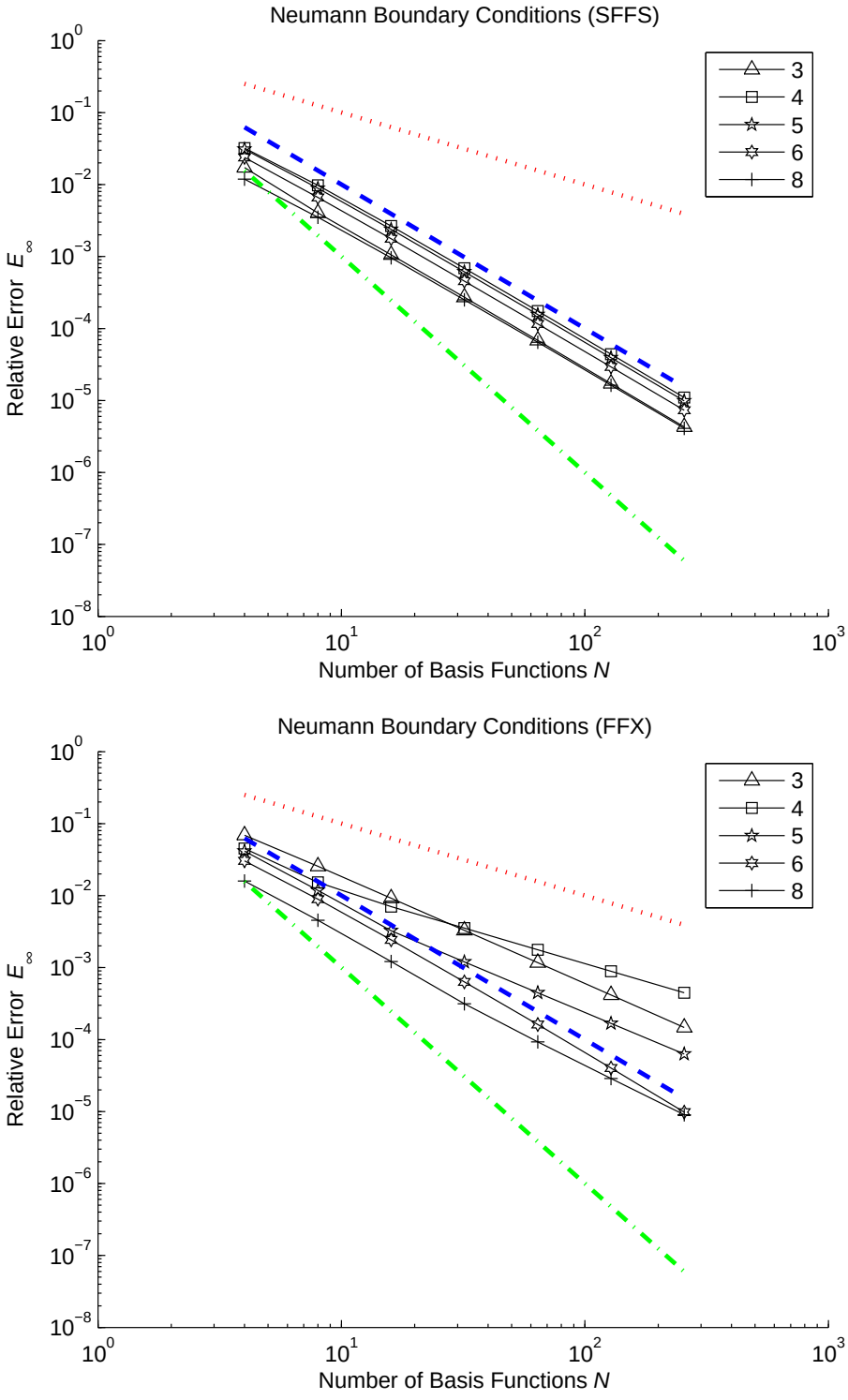

Figure 4.3 Case of regular polygons and Neumann boundary conditions : E_∞ as a function of N for the method presented here (SFFS) and the method presented in [2] (FFX)

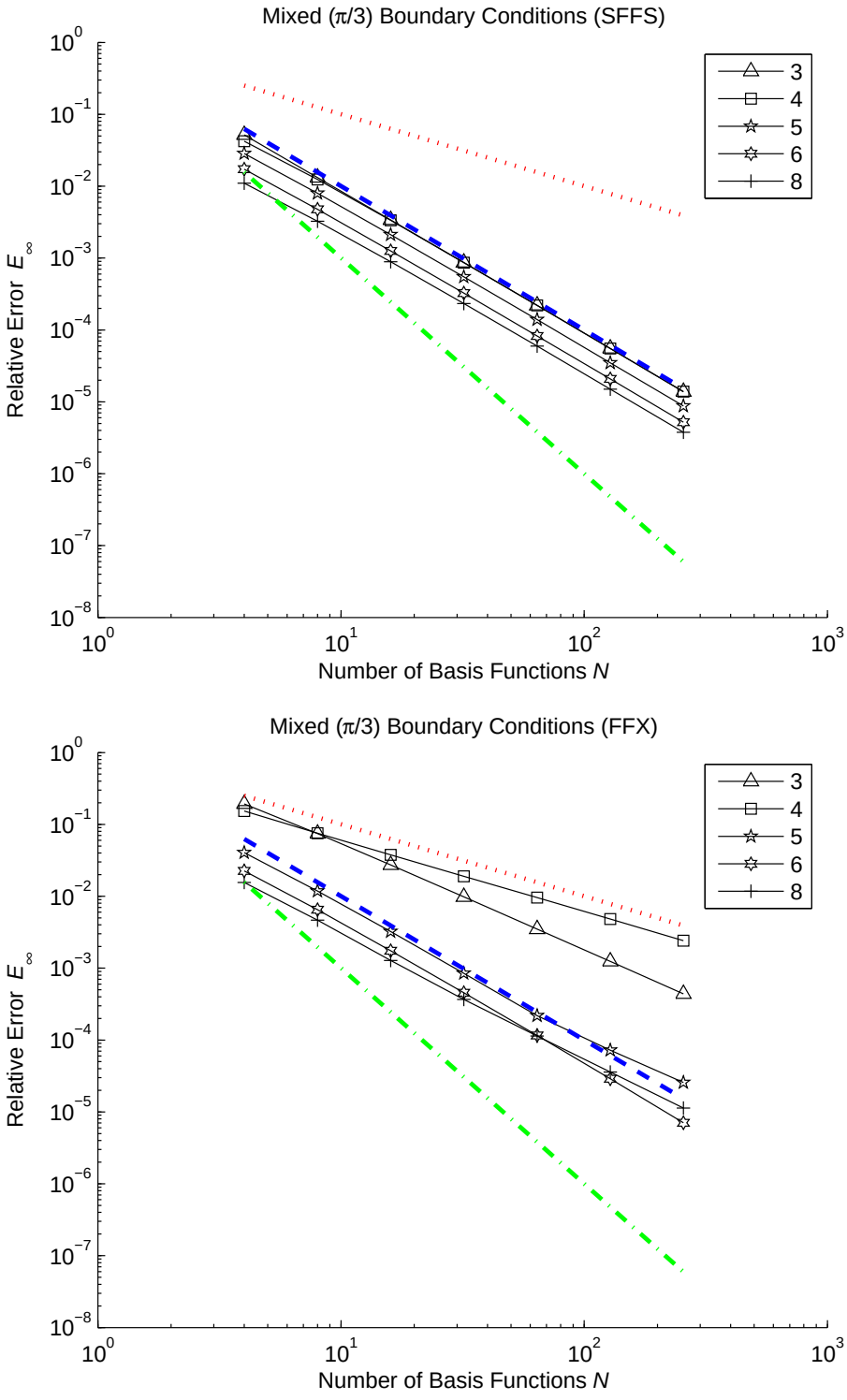

Figure 4.4 Case of regular polygons and Mixed boundary conditions : E_∞ as a function of N for the method presented here (SFFS) and the method presented in [2] (FFX)

Table 4.1 Regular Triangle - Dirichlet BCs

	SFFS method		FFX method	
N	E_∞	O.o.C	E_∞	O.o.C
4	6.94E-02	–	2.48E-01	–
8	2.04E-02	1.77	9.83E-02	1.34
16	5.44E-03	1.91	3.61E-02	1.45
32	1.40E-03	1.96	1.30E-02	1.47
64	3.56E-04	1.98	4.61E-03	1.50
128	8.96E-05	1.99	1.64E-03	1.49
256	2.25E-05	1.99	5.79E-04	1.50

Table 4.2 Regular Square - Neumann BCs

	SFFS method		FFX method	
N	E_∞	O.o.C	E_∞	O.o.C
4	3.20E-02	–	4.51E-02	–
8	9.78E-03	1.71	1.53E-02	1.56
16	2.66E-03	1.88	7.04E-03	1.12
32	6.88E-04	1.95	3.53E-03	1.00
64	1.75E-04	1.98	1.77E-03	1.00
128	4.40E-05	1.99	8.90E-04	0.99
256	1.10E-05	2.00	4.46E-04	1.00

Table 4.3 Regular Pentagon - Mixed BCs

	SFFS method		FFX method	
N	E_∞	O.o.C	E_∞	O.o.C
4	2.85E-02	–	4.04E-02	–
8	7.99E-03	1.83	1.18E-02	1.78
16	2.12E-03	1.91	3.24E-03	1.86
32	5.46E-04	1.96	8.49E-04	1.93
64	1.39E-04	1.97	2.18E-04	1.96
128	3.49E-05	1.99	7.22E-05	1.59
256	8.76E-06	1.99	2.57E-05	1.49

Table 4.4 Regular Octagon - Dirichlet BCs

	SFFS method		FFX method	
N	E_∞	O.o.C	E_∞	O.o.C
4	6.09E-03	–	1.19E-02	–
8	1.81E-03	1.75	4.37E-03	1.45
16	4.93E-04	1.88	1.47E-03	1.57
32	1.28E-04	1.95	4.79E-04	1.62
64	3.25E-05	1.98	1.54E-04	1.64
128	8.21E-06	1.98	4.88E-05	1.66
256	2.06E-06	1.99	1.54E-05	1.66

As it pertains now to the *condition number* of the coefficient matrix associated with the SFFS method we point out the fact that it remains small and grows very slowly with N in contrary to the associated condition number with the FFX method (see Figure 4.5).

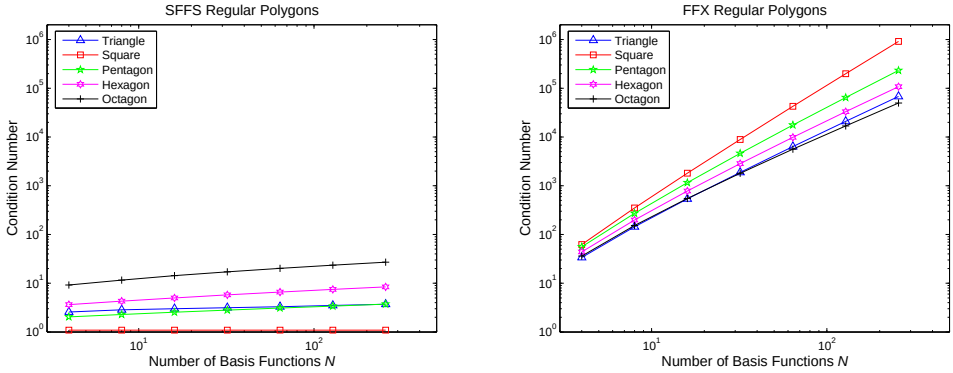

Figure 4.5 Case of regular polygons : The condition numbers of the coefficient matrices as a function of N for the method presented here (SFFS) and the method presented in [2] (FFX)

In complete analogy to the above numerical treatment, we proceed now to the numerical study of the case of *irregular polygons*. The vertices z_j of the irregular n-gons (shown in figure 4.6) used in our experiments are lying on the ellipse $\left(\frac{x}{5}\right)^2+\left(\frac{y}{2}\right)^2=1$ rotated by $\frac{1}{5}$. Their x-coordinates, before rotation, are given, in a counterclockwise

motion, by

- *Triangle* : $x = -4, -1, 3$
- *Quadrilateral* : $x = -4, 4, 4, 1$
- *Pentagon* : $x = -5, -2, 4, 3, 0$
- *Hexagon* : $x = -4, -1, 2, 4.5, 1, -4.5$
- *Octagon* : $x = -5, -4, -1, 2, 3, 1, -2, -3$

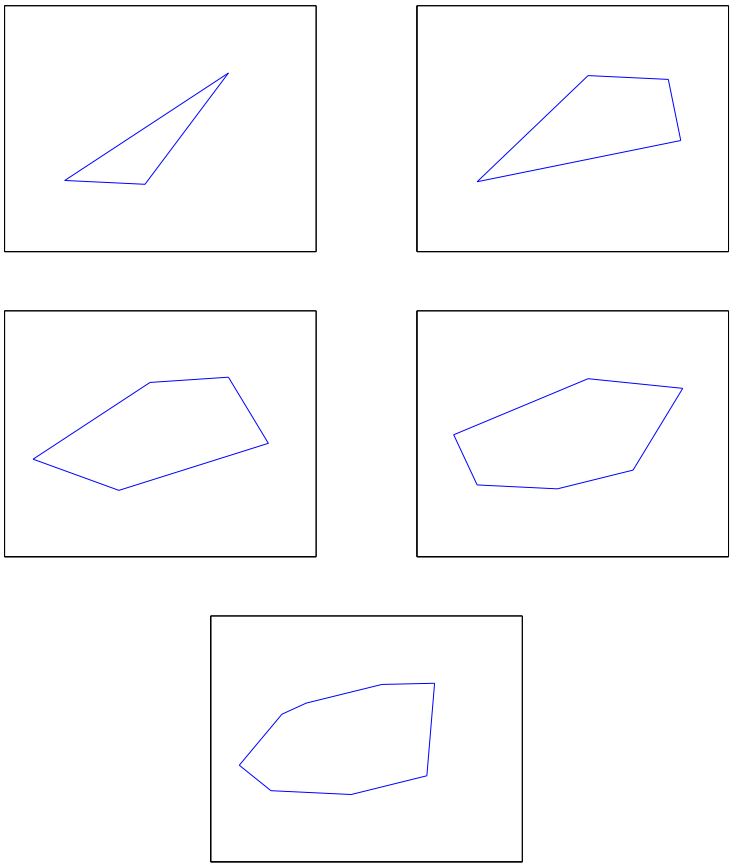

Figure 4.6 The irregular polygons used in our experiments

Figures 4.7, 4.8 and 4.9 depict the relative error E_∞ as a function of N of both SFFS and FFX methods when they apply to the solution of the discrete global relation for the case of irregular polygons with Dirichlet, Neumann and Mixed ($\beta_j = \frac{\pi}{3}$) boundary conditions respectively. Once more, both methods converge and the errors produced by the SFFS method are considerably smaller.

The quadratic convergence property of the SFFS method for the case of irregular polygons is being highlighted through Tables 4.5-4.8 that follow.

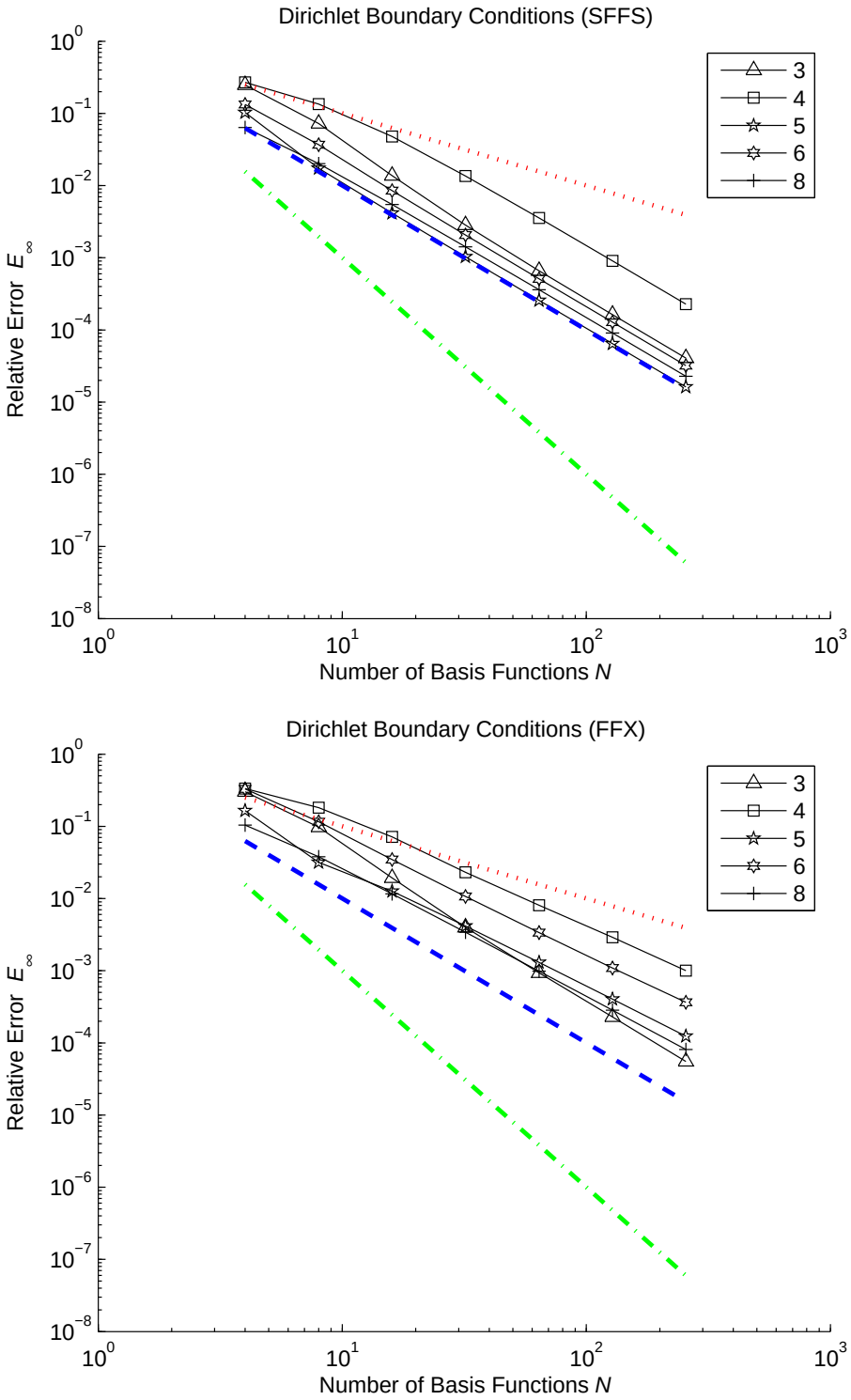

Figure 4.7 Case of irregular polygons and Dirichlet boundary conditions : E_∞ as a function of N for the method presented here (SFFS) and the method presented in [2] (FFX)

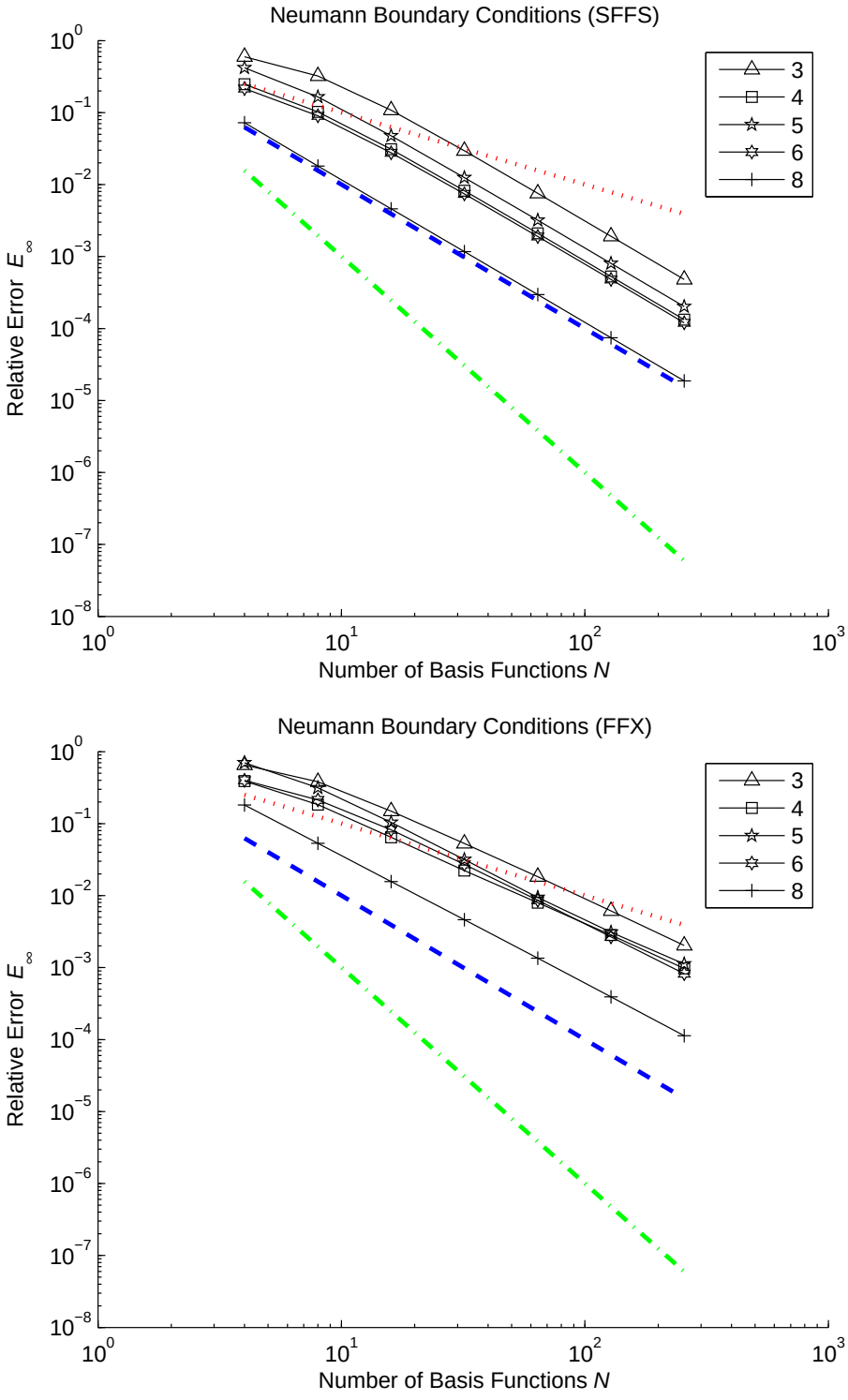

Figure 4.8 Case of irregular polygons and Neumann boundary conditions : E_∞ as a function of N for the method presented here (SFFS) and the method presented in [2] (FFX)

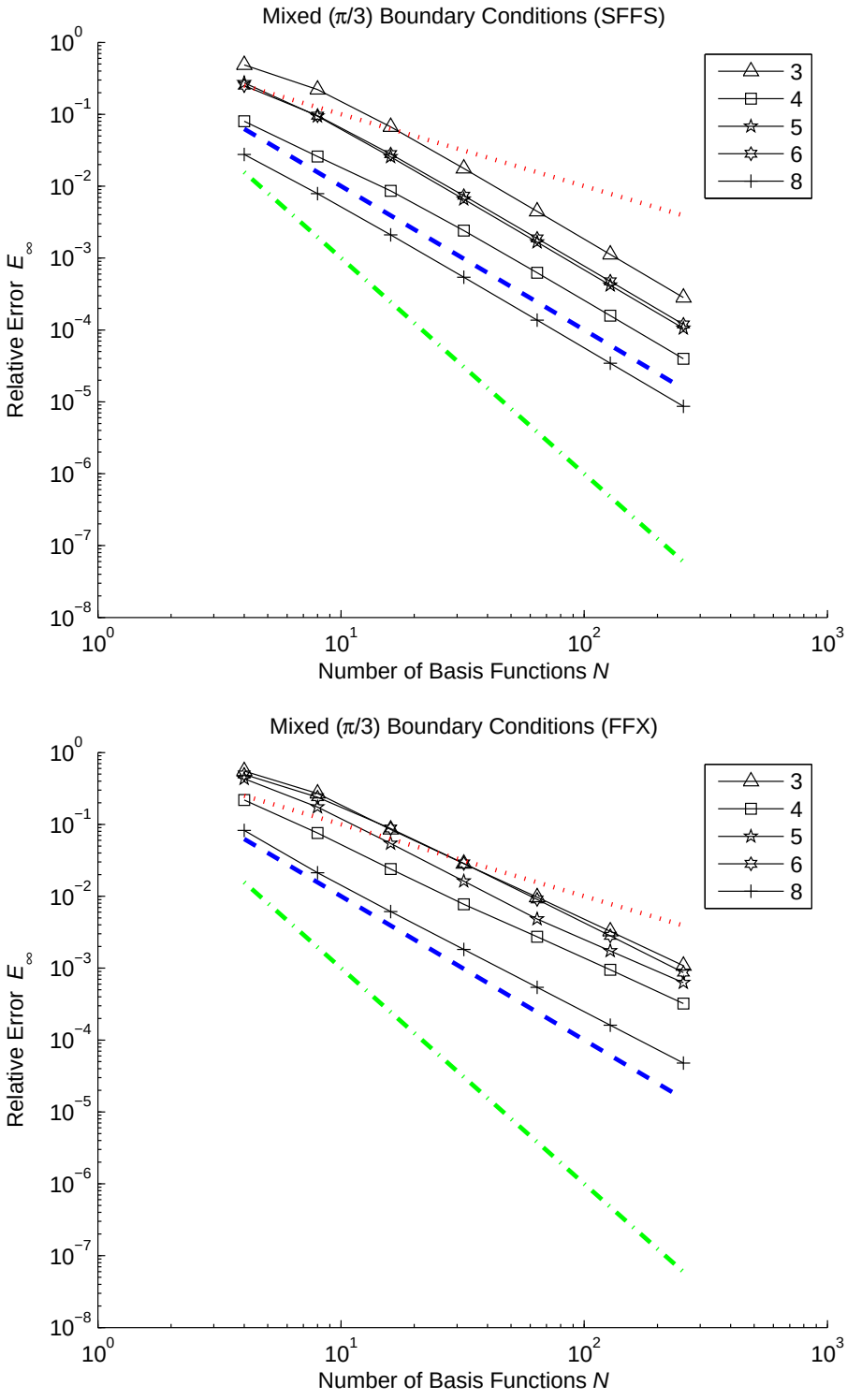

Figure 4.9 Case of irregular polygons and Mixed boundary conditions : E_∞ as a function of N for the method presented here (SFFS) and the method presented in [2] (FFX)

Table 4.5 Irregular Quadrilateral - Dirichlet BCs

	SFFS method		FFX method	
N	E_∞	O.o.C	E_∞	O.o.C
4	2.70E-01	–	3.33E-01	–
8	1.35E-01	1.00	1.81E-01	0.88
16	4.79E-02	1.49	7.13E-02	1.34
32	1.36E-02	1.82	2.31E-02	1.63
64	3.56E-03	1.93	8.05E-03	1.52
128	9.05E-04	1.98	2.90E-03	1.47
256	2.28E-04	1.99	1.00E-03	1.54

Table 4.6 Irregular Pentagon - Neumann BCs

	SFFS method		FFX method	
N	E_∞	O.o.C	E_∞	O.o.C
4	4.19E-01	–	7.01E-01	–
8	1.65E-01	1.34	3.15E-01	1.15
16	4.77E-02	1.79	1.04E-01	1.60
32	1.25E-02	1.93	3.16E-02	1.72
64	3.19E-03	1.97	9.40E-03	1.75
128	8.03E-04	1.99	3.09E-03	1.61
256	2.02E-04	1.99	1.12E-03	1.46

Table 4.7 Irregular Hexagon - Mixed BCs

	SFFS method		FFX method	
N	E_∞	O.o.C	E_∞	O.o.C
4	2.51E-01	–	4.96E-01	–
8	9.56E-02	1.39	2.39E-01	1.05
16	2.80E-02	1.77	8.74E-02	1.45
32	7.37E-03	1.93	2.86E-02	1.61
64	1.88E-03	1.97	9.04E-03	1.66
128	4.74E-04	1.99	2.81E-03	1.69
256	1.19E-04	1.99	8.69E-04	1.69

Table 4.8 Irregular Octagon - Dirichlet BCs

	SFFS method		FFX method	
N	E_∞	O.o.C	E_∞	O.o.C
4	6.38E-02	–	1.04E-01	–
8	2.01E-02	1.67	3.79E-02	1.46
16	5.48E-03	1.87	1.16E-02	1.71
32	1.42E-03	1.95	3.41E-03	1.77
64	3.60E-04	1.98	9.85E-04	1.79
128	9.07E-05	1.99	2.83E-04	1.80
256	2.28E-05	1.99	8.07E-05	1.81

Finally, Figure 4.10 refers to the behavior of the condition number of the coefficient matrices associated with the SFFS and FFX methods. Similarly to the case of regular polygons, the condition number associated with the SFFS remains small and grows very slowly with N.

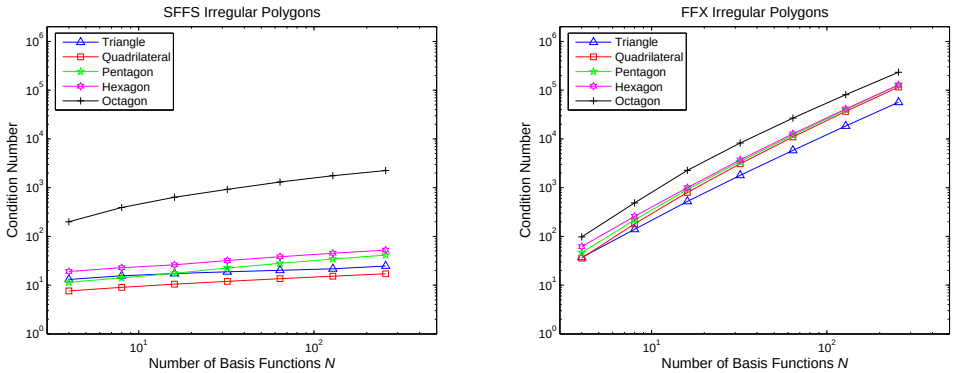

Figure 4.10 Case of irregular polygons : The condition numbers of the coefficient matrices as a function of N for the method presented here (SFFS) and the method presented in [2] (FFX)

4.2 Performance of Iterative Solution Methods for Sine Basis Functions

Here we present some preliminary results for the performance of the iterative methods employed for the solution of the linear systems produced by the two methods

(SFFS and FFX). A complete study for the behavior of iterative methods is outside the scope of the present work and will be presented elsewhere. Here we consider the classical *Jacobi* and *Gauss-Seidel* as well as the *Bi-Conjugate Gradient stabilized (BiCGstab)* iterative methods. The results depicted in Figures 4.11, 4.12 and 4.13 refer to the reduction of the relative error E_∞ with respect to the number of iterations for the regular and irregular pentagons described earlier with the number of basis functions per side fixed at $N = 64$. To improve the convergence properties of the *point* Jacobi and Gauss-Seidel iterative methods for the linear system produced by the method in [2], we also considered their *block* analogs (the block size is fixed to N). For the same reason, together with the *unpreconditioned* BiCGstab we have also considered its *block Jacobi preconditioned* analog. In these cases, the computational cost increases due to the factorization involved. The maximum number of iterations allowed for all methods to perform is set to 200 and the zero iterate $U^{(0)}$ is set to be equal to the right hand side vector. The stopping criterion used for the Jacobi and Gauss-Seidel methods is

$$E_\infty^{(1)} = \frac{||U^{(m+1)} - U^{(m)}||_\infty}{||U^{(m+1)}||_\infty} \ \leq \ 10^{-6} \ ,$$

while for the BiCGstab method is

$$E_\infty^{(2)} = \frac{||b - AU^{(m)}||_\infty}{||b||_\infty} \ \leq \ 10^{-6} \ ,$$

where A, b and $U^{(m)}$ denote the coefficient matrix (with the appropriate modifications for the preconditioned cases), the right hand side vector and the $m-th$ iterate respectively.

Figures 4.11-4.13 indicate the following :

- All iterative methods for the SFFS-algorithm converge rapidly in a few iterations. Specifically, for the case of the regular pentagon the Jacobi, Gauss-Seidel and BiCGstab iterative methods converge in 9, 7 and 4 iterations respectively. For the case of the irregular pentagon the corresponding numbers of iterations are 30, 16 and 7 respectively.

- The same iterative methods for the FFX-algorithm appear to have weak convergent properties. Namely, the Jacobi method diverges and the unpreconditioned BiCGstab method fails to reduce the relative error $E_\infty^{(2)}$ to a value less than 10^{-6} after 200 iterations for both cases of regular and irregular pentagons. The Gauss-Seidel method converges in 69 and 125 iterations for the case of regular and irregular pentagons respectively. The situation improves by using the block Jacobi and Gauss-Seidel as well as the block Jacobi preconditioned BiCGstab methods, but this leads to extra computational cost due to the direct factorization involved. In these cases, the iterations needed for the convergence of the block-Jacobi, block-Gauss-Seidel and preconditioned-BiCGstab methods respectively are 46, 24 and 10 for the regular pentagon and 34, 21 and 10 for the irregular pentagon.

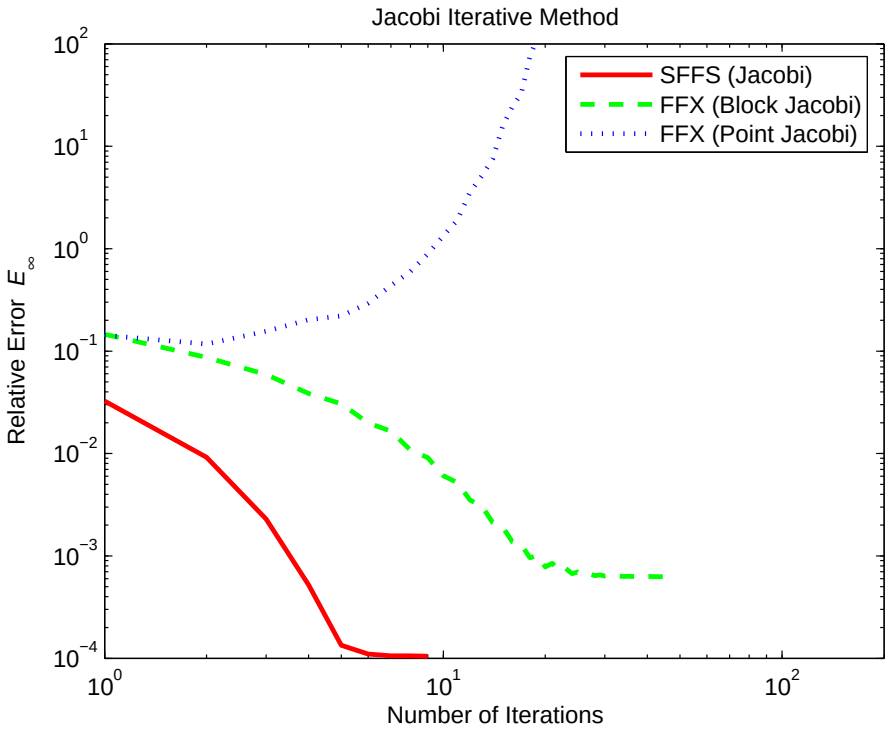

(a)

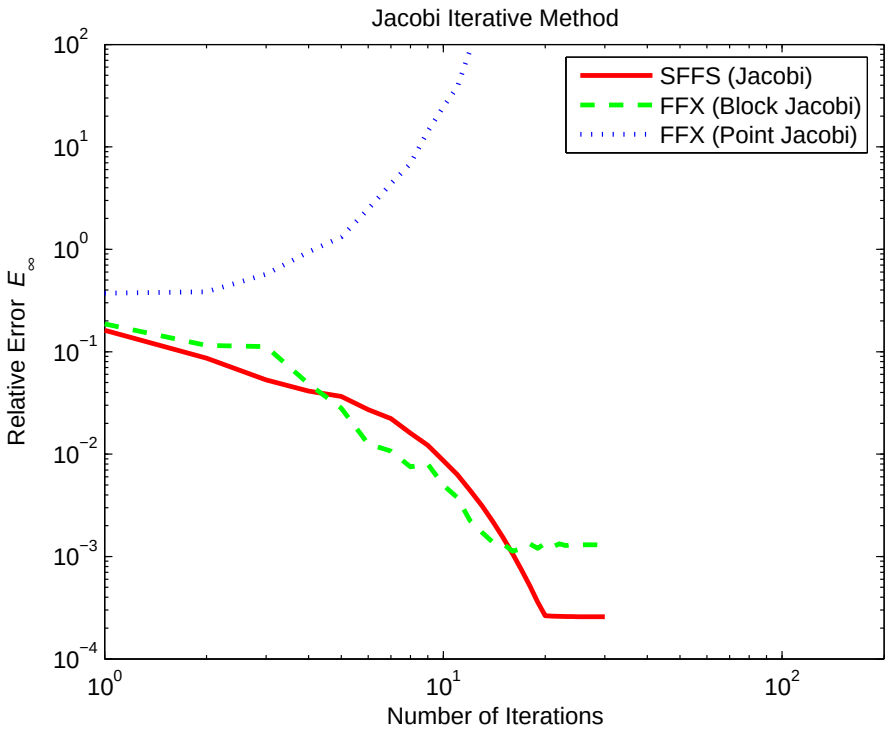

(b)

Figure 4.11 The relative error E_∞ as a function of Jacobi iterations for a (a) regular and an (b) irregular pentagon ($N = 64$)

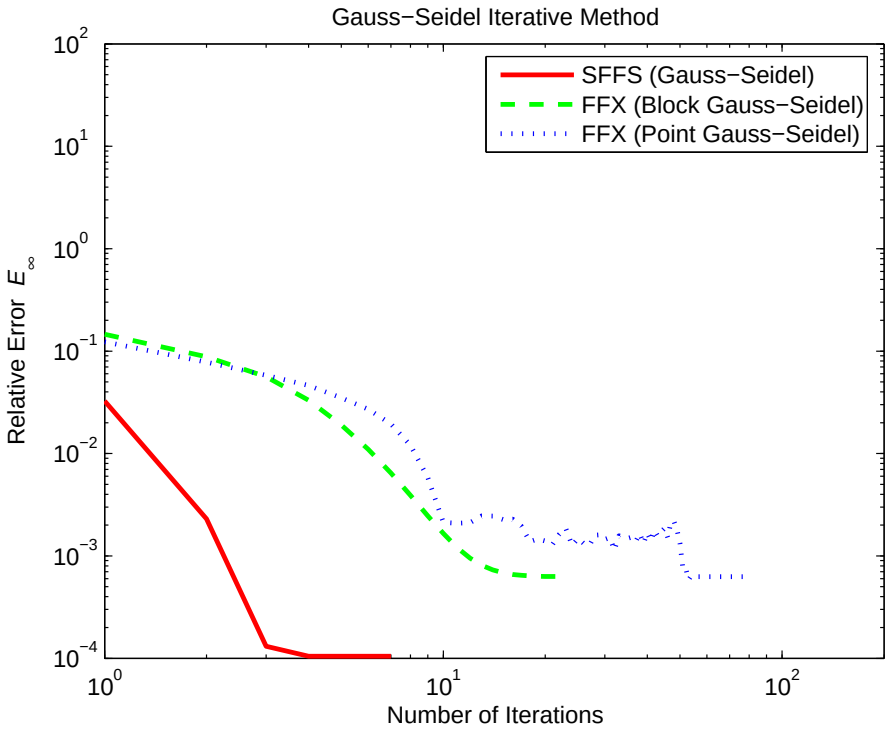

(a)

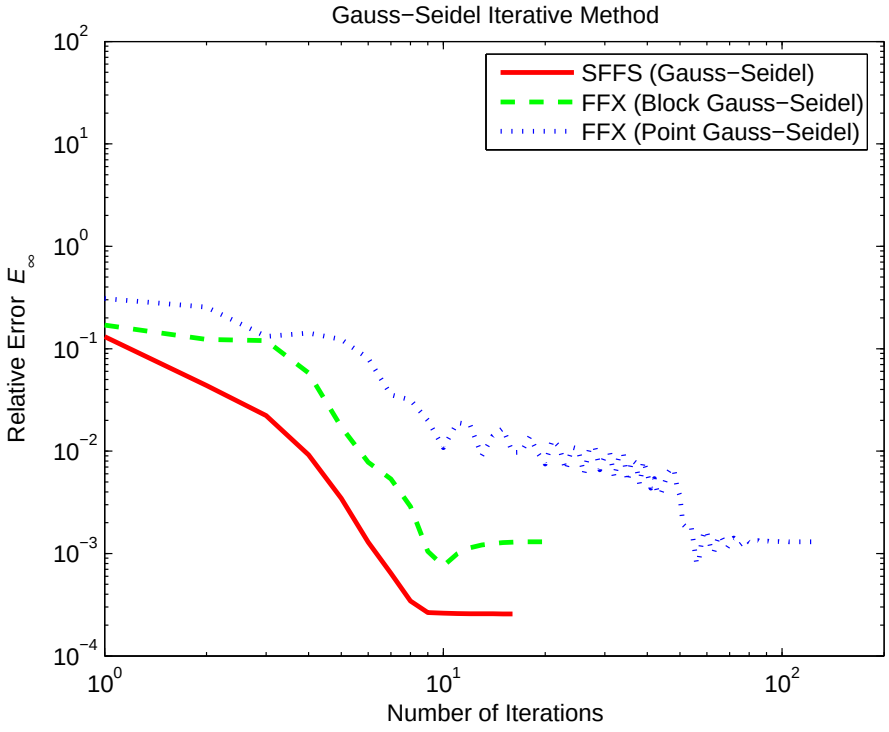

(b)

Figure 4.12 The relative error E_∞ as a function of Gauss-Seidel iterations for a (a) regular and an (b) irregular pentagon ($N = 64$)

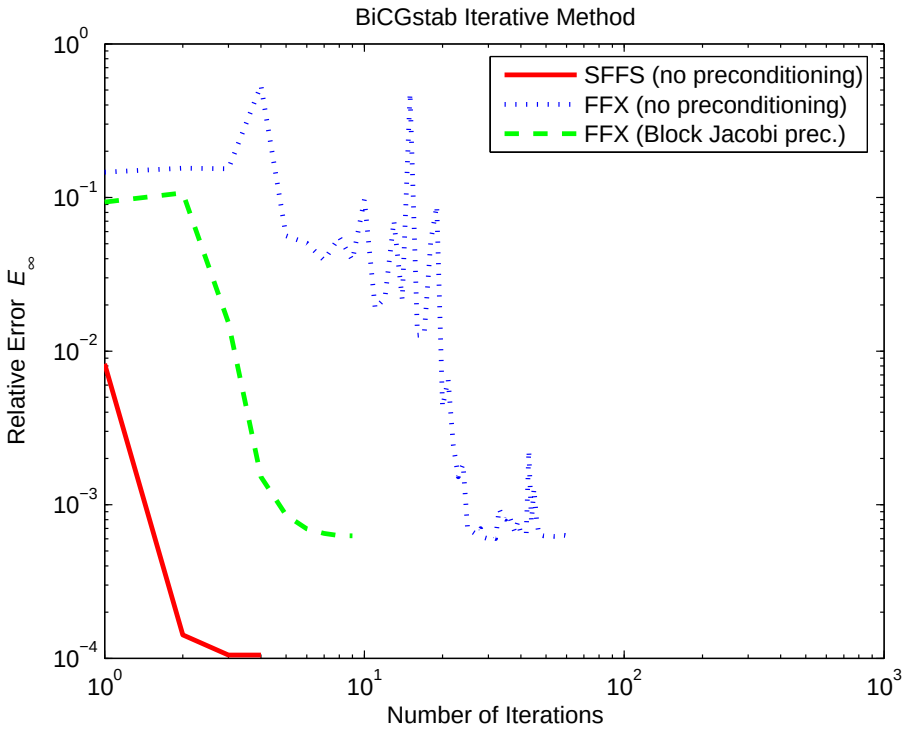

(a)

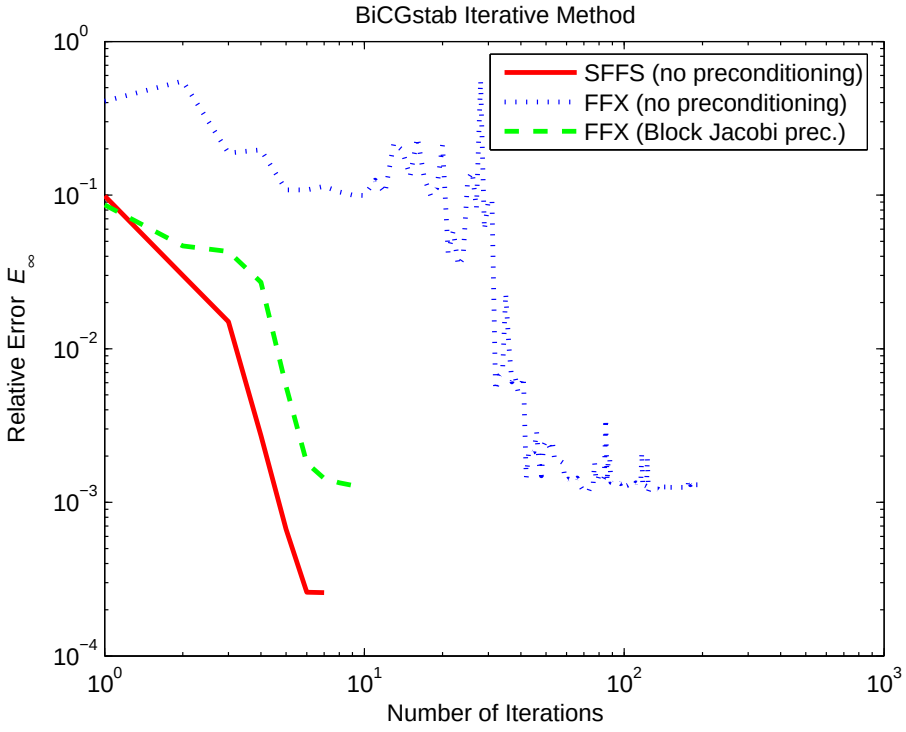

(b)

Figure 4.13 The relative error E_∞ as a function of BiCGstab iterations for a (a) regular and an (b) irregular pentagon ($N = 64$)

The sine basis functions $\varphi_r(s)$ used in the approximation (3.1) in both the SFFS and FFX methods are natural in that they are closely connected to the underlying Fourier transform [cf. (3.4)]. Indeed, this is the reason that the diagonal blocks in the matrix are diagonal. However, from the point of view of approximation theory, these functions are not optimal. Thus, we can ask: can the convergence be improved by using other basis functions? Here we explore only one choice, namely, polynomials. Since the endpoint values of the unknown functions $f^{(j)}$ have been removed (see Remark 2.3 above), the basis functions should vanish at the endpoints $s = \pm\pi$. To obtain reasonable conditioning, we construct polynomial basis functions from the Chebyshev polynomials $T_n(x) = \cos\left(n\cos^{-1}(x)\right)$, defining $\varphi_r(s)$ for $r = 1, \ldots, N$ by

$$\varphi_r(s) = \begin{cases} T_{r+1}\left(\frac{s}{\pi}\right) - T_0\left(\frac{s}{\pi}\right), \; r \text{ odd}, \\ \\ T_{r+1}\left(\frac{s}{\pi}\right) - T_1\left(\frac{s}{\pi}\right), \; r \text{ even}. \end{cases}$$

The Fourier transforms of these functions needed for (3.4) can be computed using the recursion relation

$$2T_n(x) = \frac{T'_{n+1}(x)}{n+1} - \frac{T'_{n-1}(x)}{n-1}, \qquad n > 1.$$

Figures 4.14–4.16 show the error E_∞ as a function of N for the SFFS method using this Chebyshev basis for the regular and irregular polygon cases of section 4.1. In each case the convergence is faster than quadratic; for the regular polygons, it appears to be exponential. The convergence is slower for the irregular polygons; the eventual breakdown of convergence may be due to roundoff error. In each case the error for a given value of N is smaller than that obtained with the sine basis. While the diagonal blocks in the linear system are no longer diagonal, the matrices are still well-conditioned, with condition numbers (not shown) typically less than 10 until the convergence breaks down.

5 Conclusions and Remarks

We have introduced a revised implementation of the *collocation* numerical method introduced in [2] for solving linear elliptic PDEs with constant coefficients on arbitrary polygonal domains. The new version is based on a different choice of *"collocation points"*, as well as different choice of basis functions and produces significantly better approximations, especially for regular polygons. This is numerically demonstrated in section 4, however a rigorous proof for the convergence remains open. The associated condition number for polygons with relatively few number of sides remains confined and smaller than the corresponding one in [2].

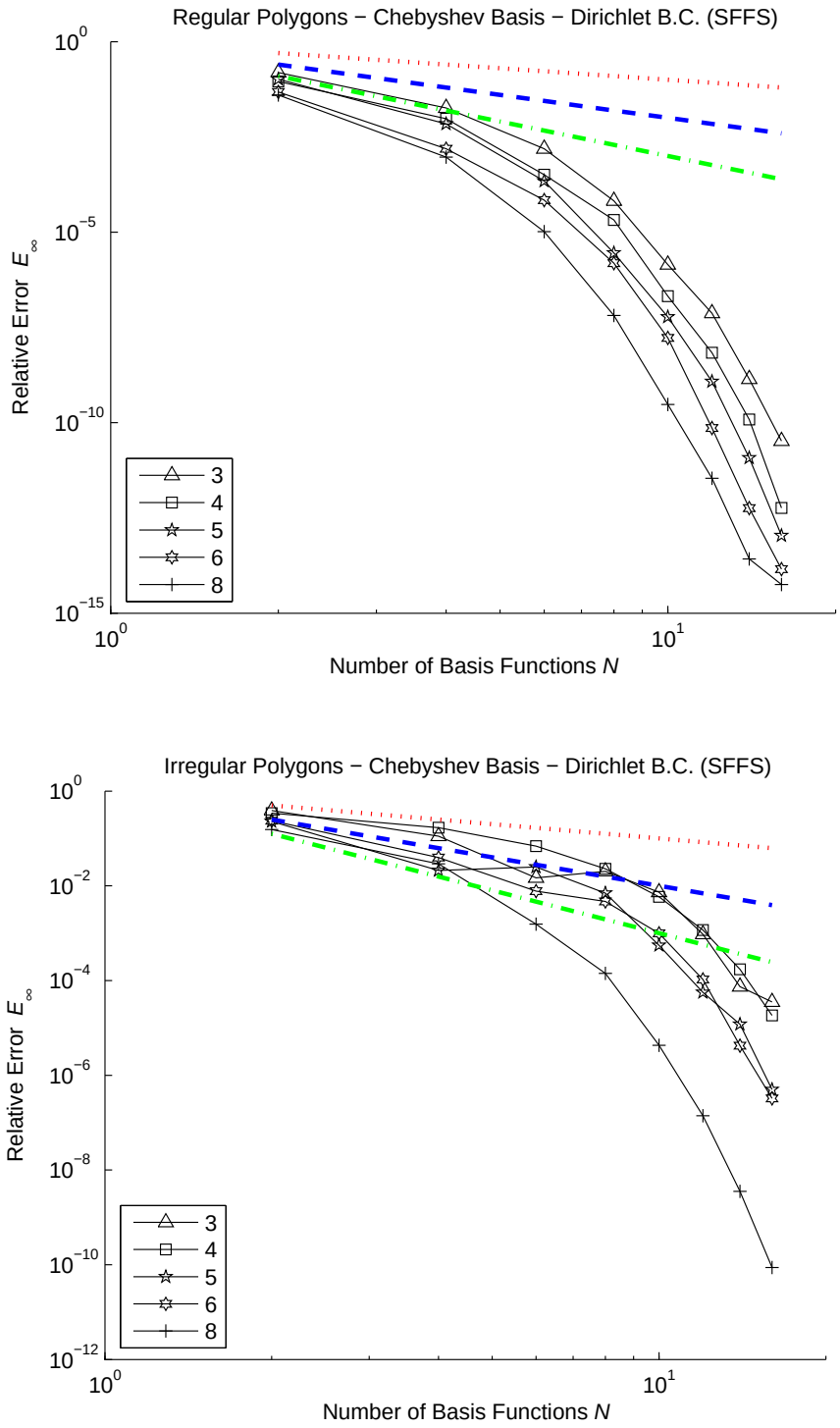

Fig. 4.14. E_∞ as a function of N for the SFFS method with Chebyshev basis functions for regular polygons (top panel) and irregular polygons (bottom panel) with Dirichlet boundary conditions.

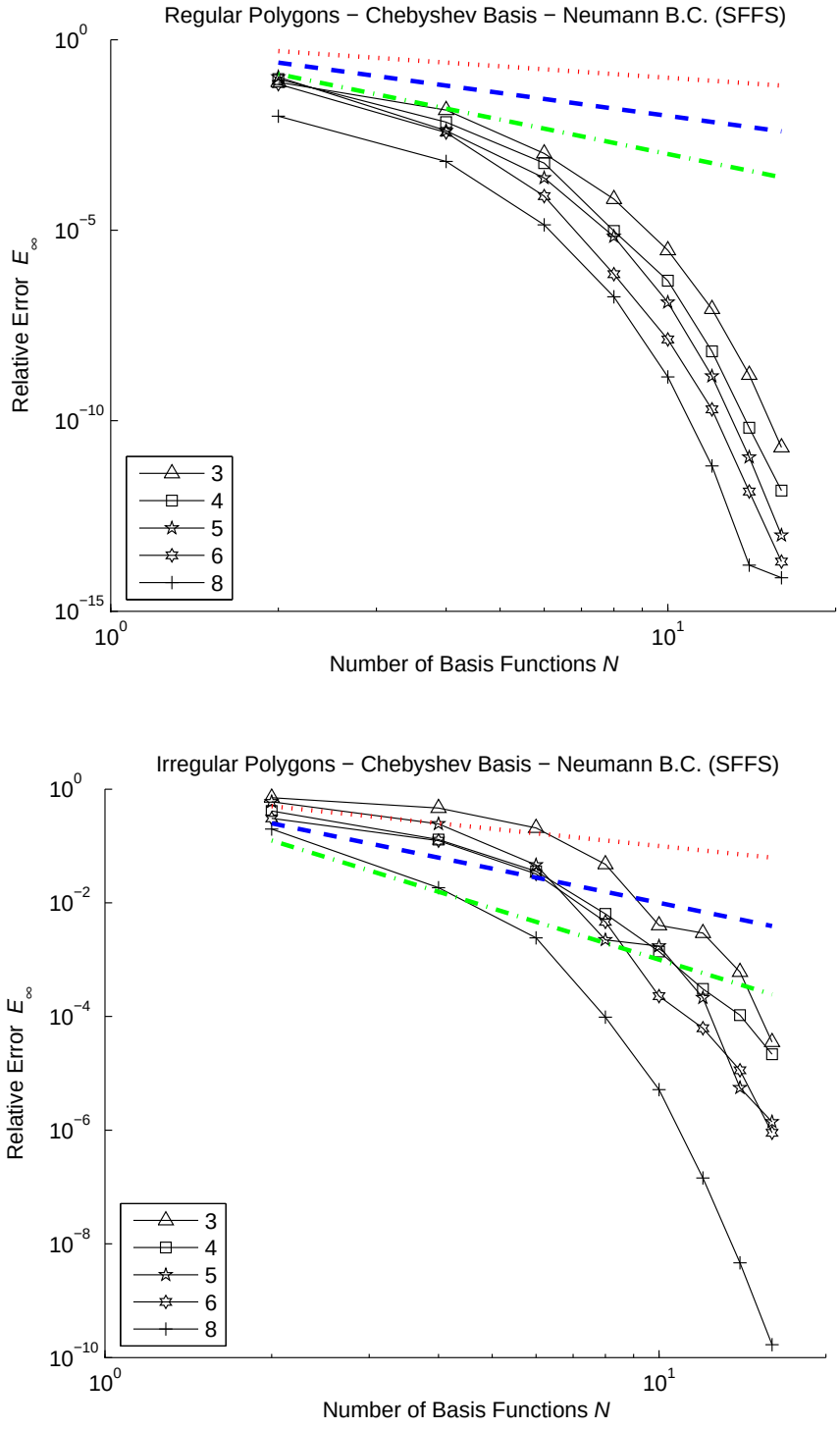

Fig. 4.15. E_∞ as a function of N for the SFFS method with Chebyshev basis functions for regular polygons (top panel) and irregular polygons (bottom panel) with Neumann boundary conditions.

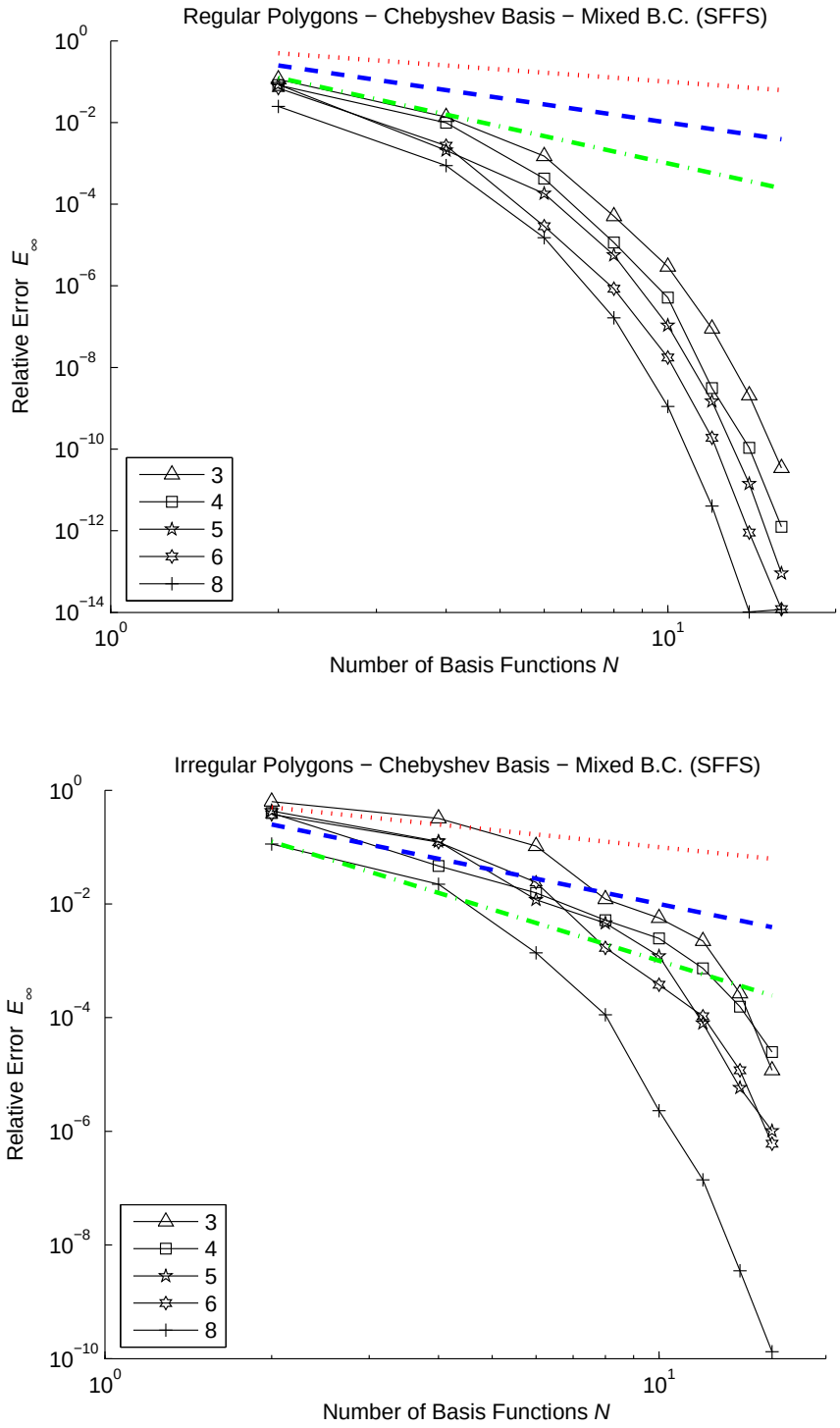

Fig. 4.16. E_∞ as a function of N for the SFFS method with Chebyshev basis functions for regular polygons (top panel) and irregular polygons (bottom panel) with mixed $(\pi/3)$ boundary conditions.

For the case of sine basis functions, the computational advantage of our method is based on the fact that the block diagonal submatrices of the coefficient matrix of the linear system obtained from the discrete analog of the *global relation* (cf. [1], [3]), are strictly diagonal. Thus, by construction and without introducing any computational cost from direct factorization, the coefficient matrix is *"block-Jacobi preconditioned"*. This property, besides the fact that it can be used to reduce the computational cost of direct factorization methods, points directly to the efficient implementation of the classical *SOR-like* and *CG-like* iterative methods. The rapid convergence properties of the Jacobi, Gauss-Seidel and BiCGstab iterative methods are numerically demonstrated in the previous section for regular and irregular pentagons. A complete numerical study for the behavior of iterative methods pertaining to our algorithm, as well as their rigorous convergence analysis, is in progress.

For the case of Chebyshev basis functions, the block diagonal submatrices are no longer diagonal matrices, but the condition number is still small and numerical experiments indicate higher order of convergence. In particular, for regular polygons, it appears that the method converges exponentially.

This new method has been implemented recently to the Modified Helmholtz and to the Helmholtz equations in the interior of a convex polygon.

References

[1] A.S.Fokas, A unified transform method for solving linear and certain nonlinear PDEs, *Proc. R. Soc. London A***53** (1997), 1411-1443.

[2] S. Fulton, A.S. Fokas and C. Xenophontos, An Analytical Method for Linear Elliptic PDEs and its Numerical Implementation, *J. of Comput. and Appl. Maths.* **167** (2004), 465-483.

[3] A.S.Fokas, Two-dimensional linear PDEs in a convex polygon, *Proc. R. Soc. London A* **457** (2001), 371-393.

[4] A.S. Fokas, A New Transform Method for Evolution PDEs, *IMA J. Appl. Math.* **67** (2002), 559.

[5] A.S. Fokas and B. Pelloni, A Transform Method for Evolution PDEs on the Interval, *IMA J. Appl. Math.* (2005), 1-24.

[6] D. ben-Avraham and A.S. Fokas, The Modified Helmholtz Equation in a Triangular Domain and an Application to Diffusion-limited Coalescence, *Phys. Rev. E* **64** (2001), 016114-6.

[7] Y.A. Antipov and A.S. Fokas, A Transform Method for the Modified Helmholtz Equation in a Semi-Strip, *Math. Proc. Camb. Phil. Soc.* **138** (2005), 339-365.

[8] G. Dassios and A.S. Fokas, The Basic Elliptic Equations in an Equilateral Triangle, *Proc. R. Soc. Lond.* **A 461** (2005), 2721-2748.

[9] D. Crowdy and A.S. Fokas, Explicit Integral Solutions for the Plane Elastostatic Semi-Strip, *Proc. R. Soc. Lond.* **460** (2004), 1285-1309.

[10] A.S. Fokas, Integrable Nonlinear Evolution Equations on the Half-Line, *Comm. Math. Phys.* **230** (2002), 1-39.

[11] A.S. Fokas, Linearizable Initial Boundary Value Problems for the sine-Gordon Equation on the Half-Line, *Nonlinearity* **17** (2004), 1521-1534.